Faster decline and higher variability in the sea ice thickness of the marginal Arctic seas

Robbie D.C. Mallett [1], Julienne C. Stroeve [1,2,3], Michel Tsamados [1], Jack C. Landy [4], Rosemary Willatt [1], Vishnu Nandan [3], and Glen E. Liston [5]

[1]Centre for Polar Observation and Modelling, Earth Sciences, University College London, London, UK
[2]National Snow and Ice Data Center, University of Colorado, Boulder, CO, USA
[3]Centre for Earth Observation Science, University of Manitoba, Winnipeg, Canada
[4]School of Geographical Sciences, University of Bristol, Bristol, UK
[5]Cooperative Institute for Research in the Atmosphere, Colorado State University, Fort Collins, CO, USA

Correspondence: Robbie Mallett (robbie.mallett.17@ucl.ac.uk)

Abstract. Mean sea ice thickness is a sensitive indicator of Arctic climate change and in long-term decline despite significant interannual variability. Current thickness estimations from satellite radar altimeters employ a snow climatology for converting range measurements to sea ice thickness, but this introduces unrealistically low interannual variability and trends. When the sea ice thickness in the period 2002-2018 is calculated using new snow data with more realistic variability and trends, we find

5 mean sea ice thickness in three of the seven marginal seas to be declining between 70-100% faster than when calculated with the conventional method. When analysed as an aggregate, the mean ice thickness in the marginal seas is now in statistically significant decline for four of seven winter months. This is observed despite a 58% increase in interannual variability between the methods in the same time period. On a seasonal timescale we find that snow data exerts an increasingly strong control on thickness variability over the growth season, contributing only 20% in October but 72% by April. Higher variability and faster

10 decline in the sea ice thickness of the marginal seas has wide implications for our understanding of the polar climate system and our predictions for its change, as well as for stakeholders involved in Arctic shipping and natural resource extraction.

1 Introduction

Sea ice cover moderates the exchange of moisture, heat and momentum between the atmosphere and the polar oceans, influencing regional ecosystems, hemispheric weather patterns and global climate. Sea ice thickness (SIT) is a key characteristic of

15 the sea ice cover, as thicker ice weakens the coupling between the ocean and atmosphere systems.

Thicker ice is more thermally insulating and limits heat transfer from the ocean to the atmosphere in winter and consequent thermodynamic growth (Petty et al., 2018a). SIT also exerts control on ice dynamics and rheology (Tsamados et al., 2013); for instance, it determines whether floes ridge or raft when pressed against each other (Vella and Wettlaufer, 2008). The thickness of sea ice during snow accumulation also dictates whether the ice surface drops below the waterline, potentially increasing

20 thermodynamic ice growth through the formation of snow-ice (Rösel et al., 2018). The impact of the end-of-winter SIT distribution persists into the melt season with thin ice favoring melt-pond formation, and thick ice decreasing the transmission

of solar radiation to the surface ocean and reducing the potential for in- and under-ice primary productivity (Mundy et al., 2005; Katlein et al., 2015). Finally, thick ice is far more likely to survive the melt season, increasing the average age of Arctic sea ice and offering opportunities for prediction of the sea ice state on seasonal timescales (Chevallier and Salas-Mélia, 2012;
25 Blockley and Peterson, 2018; Schröder et al., 2019).

The annual sea ice thickness distribution is highly spatially variable, with a cover of thick multi-year ice in the Central Arctic and a thinner, more seasonally variable cover of first year ice in the marginal seas. Regional sea ice thickness distributions are often characterised by the mean thickness, $\overline{SIT}$. As well as being a key parameter for the processes described above, the value can be multiplied by the sea ice area to produce the sea ice volume, one of the most sensitive indicators of Arctic climate
30 change (Schweiger et al., 2019).

While continuous and consistent monitoring of Pan-Arctic SIT has not been achieved on a multi-decadal timescale, a combination of different techniques has suggested a significant decline in thickness since 1950 (Kwok, 2018; Stroeve and Notz, 2018). Satellite altimeters using both radar and lidar have provided a valuable record of changing sea ice thickness, but have often been limited for various reasons. Some have been limited spatially by their orbital inclination (e.g. the ERS, Envisat, AltiKa
35 and Sentinel radar altimeters have operated up to only 81.5 degrees north), and others in temporal coverage (e.g. ICESat was operated in 'campaign mode' rather than providing continuous coverage). Two satellite altimeters currently offer continuous and meaningfully Pan-Arctic monitoring of the Arctic sea ice: the ICESat-2 and CryoSat-2 altimeters. ICESat-2 has been in operation since September 2018 and so far has documented only two winters of sea ice thickness (Kwok et al., 2020).

Although the launch of the CryoSat-2 radar altimeter (henceforth CS2) in 2010 allowed significant advances in understanding
40 the spatial distribution and interannual variability of Pan-Arctic SIT (Laxon et al., 2003), a statistically significant decreasing trend within the CS2 observational period has not been detected for the Arctic as a whole. The lack of certainty regarding any trend in SIT is in part due to the various uncertainties associated with SIT retrieval from radar altimetry (Ricker et al., 2014; Zygmuntowska et al., 2014). Major contributors to these uncertainties are the relatively large footprint of a radar pulse when compared to laser altimetry, the variable density of sea ice, retracking of radar returns from rough ice, and the need for an *a*
45 *priori* snow depth and density distribution (Kern et al., 2015; Landy et al., 2020).

The impact of snow-depth uncertainty on SIT retrievals was recently included by the IPCC in a list of 'Key Knowledge Gaps and Uncertainties' (Meredith et al., 2019). More specifically, Bunzel et al. (2018) found snow to have a strong influence on the interannual variability of SIT and consequent detection of thickness trends. Here we investigate the impact of a new, Pan-Arctic snow depth and density data set (SnowModel-LG; Liston et al., 2020; Stroeve et al., 2020) on trends and variability
50 in regional $\overline{SIT}$ when used in place of the traditional, climatological data set (Warren et al., 1999). We show that traditional calculations of $\overline{SIT}$ omit significant interannual variability due to their reliance on a snow climatology, and we quantify this omission. We also show that sea ice is likely thinning at a faster rate in some marginal seas than previously thought, because the snow water equivalent on the ice is declining too.

1.1 The Role of Snow in Radar-Altimetry Derived Sea Ice Thickness Retrievals

55 Satellite radar altimetry involves the emission of radar pulses from a satellite and the subsequent detection of their backscatter. The time difference between emission and detection ('time of flight') corresponds to the distance traveled and thus the height of the transmitter above the scattering surface. Radar altimeters of different frequencies have been carried on board several earth observation satellites such as ERS-1/2, Envisat, AltiKa, CryoSat-2 and Sentinel-3A/B (Quartly et al., 2019). We now quantify the role of snow cover in conventional sea ice thickness estimation, before revealing and explaining the effects of previously 60 unincorporated trends and variability.

The Ku-band radar waves emitted from CryoSat-2 are generally assumed in mainstream SIT products to scatter from the snow/sea-ice interface (Kurtz et al., 2014; Tilling et al., 2018; Hendricks and Ricker, 2019; Landy et al., 2020). The difference in radar ranging (derived from time-of-flight) between areas of open water and areas of sea ice is known as the 'radar freeboard', f_r. The height of the ice surface above the waterline is referred to as the ice freeboard, f_i. This is extracted from the radar 65 freeboard through (a) assuming that the primary scattering horizon corresponds to the ice surface, and (b) accounting for the slower radar wave propagation through the snow cover above the ice surface (Armitage and Ridout, 2015; Mallett et al., 2020). The ice freeboard can then be converted to ice thickness by considering the floe's hydrostatic equilibrium given the ice density and weight of overlying snow. In the simplified case of bare ice, we would calculate:

$$SIT_{bare} = f_r \frac{\rho_w}{\rho_w - \rho_i} \tag{1}$$

70 Where ρ_w is the density of seawater and ρ_i the density of ice. We now identify that the height correction due to slower radar propagation in snow scales in almost directly proportion to the total mass of penetrated snow (m_s; Fig. S1). As such, it can be easily combined with the change to the floe's hydrostatic equilibrium from snow loading (also linearly dependent on m_s) to make one transformation to modify the function $SIT_{bare} = g(f_r)$ for a known mass of overlying snow $SIT = h(f_r, m_s)$:

$$SIT = f_r \frac{\rho_w}{\rho_w - \rho_i} + m_s \frac{\rho_w}{\rho_w - \rho_i} \times 1.81 \times 10^{-3} \tag{2}$$

75 Physically, the first term of Eq. (2) corresponds to the SIT were the ice known to have no snow cover. The second term is the additional thickness of ice below the waterline that is inferred from knowledge of the overlying snow cover. SIT has been decomposed into linearly independent contributions from radar-freeboard data and snow data. This allows the contributions of the two data components to SIT to be assessed independently. A derivation of the 1.81×10^{-3} coefficient is available in the supplementary material.

80 Eq. (2) and its factor of 1.81×10^{-3} allow the simple expression of the theoretical change to the radar freeboard under rapid snow accumulation or removal. Making f_r the subject of the equation and assuming SIT constant we find:

$$\frac{\partial f_r}{\partial m_s} = -1.81 \times 10^{-3} \quad (m/kgm^{-2}) \tag{3}$$

We stress that the above equation assumes total radar penetration of overlying snow, an assumption discussed in Sect. (5.2.2). As well as allowing independent analysis of the radar and snow data contributions to SIT at a point, the linearly independent

85   nature of Eq. (2) in terms of f_r and m_s allows for a simple calculation of the average SIT in a region ($\overline{SIT}$) as:

$$\overline{SIT} = \overline{RF} + \overline{Snow} \tag{4}$$

Where $\overline{RF}$ and $\overline{Snow}$ represent the spatial averages of the first and second terms of Eq. (2). Sect. (4.1) of this paper focuses on the interannual variability in $\overline{SIT}$ which (treating $\overline{RF}$ and $\overline{Snow}$ as random, dependent variables) can be expressed thus:

$$\sigma^2_{\overline{SIT}} = \sigma^2_{\overline{RF}} + \sigma^2_{\overline{Snow}} + 2\,\mathrm{Cov}(\overline{RF}, \overline{Snow}) \tag{5}$$

90   Where the final term represents the covariance between spatially averaged radar freeboard and snow contributions. This covariance term can be expressed as $2\rho \times \sigma_{\overline{SIT}} \times \sigma_{\overline{RF}}$, where ρ is the dimensionless correlation-coefficient between the variables and ranges between -1 and 1. To further explain this term, if years of high $\overline{RF}$ are correlated with high $\overline{Snow}$, then the covariance term will be high and interannual variability in $\overline{SIT}$ will be amplified. If mean snow depths are anti-correlated with mean radar freeboard across the years, interannual variability in $\overline{SIT}$ will be reduced.

95   Detection of temporal trends in $\overline{SIT}$ is critically dependent on accurate characterisation of $\sigma^2_{\overline{SIT}}$. This is because conventional tests for trend exploit the known probability of a system with no trend generating the data at hand through variability alone (Chandler and Scott, 2011, p. 61). In this paper we argue that the $\sigma^2_{\overline{Snow}}$ term of Eq. (5) has been systematically underestimated through the use of a quasi-climatological snow data set. As an alternative to this we use the results of SnowModel-LG, a snow accumulation model that incorporates interannual changes in precipitation amount, freeze-up timing and ice distribution.

100   Before examining the impacts of the SnowModel-LG data on the $\overline{SIT}$ timeseries, we briefly survey the snow climatology given by Warren et al. (1999) and its implementation in SIT retrievals.

1.2   The Warren Snow Climatology for SIT Retrieval

The most commonly used radar-altimetry SIT products use algorithms developed by the Centre for Polar Observation and Modelling, the Alfred Wegener Institute and the NASA Goddard Space Flight Centre (Tilling et al., 2018; Hendricks and

105   Ricker, 2019; Kurtz et al., 2014). Another commonly used but not publicly available product is from the NASA Jet Propulsion Laboratory (Kwok and Cunningham, 2015). All four groups utilize modified forms of the snow climatology assembled from the observations of Soviet drifting stations between 1954 and 1991 (Warren et al., 1999, Henceforth W99).

We highlight here that our expression of the contribution of snow data to SIT solely in terms of snow mass (Eq. 2) is technically convenient for using W99 to estimate sea ice thickness, as quadratic fits of depth and snow water equivalent (SWE)

110   are published without corresponding fits of density. Density values previously required for correcting for radar speed in snow are often set to a constant value or 'backed out' by dividing the published SWE distributions by the depth distributions, compounding uncertainties in sea ice thickness.

While the consistent use of W99 for sea ice thickness calculation is convenient for intercomparison of products (e.g. Sallila et al., 2019; Landy et al., 2020), the data have a number of drawbacks. This work is centered around two key issues with the

115   use of W99 for SIT retrieval: inadequate representation of interannual variability and trends.
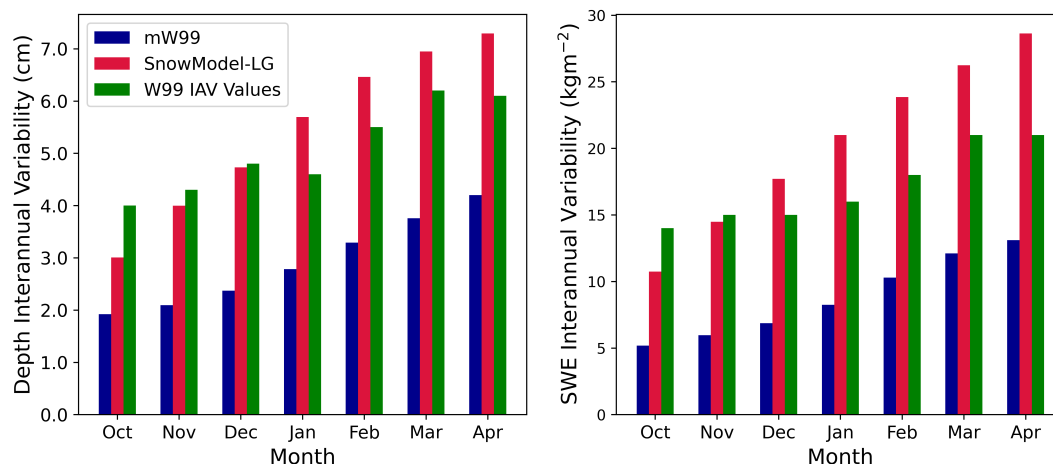
Figure 1. Interannual variability (2002-2018) in snow depth from mW99 and SnowModel-LG compared to the values given in Table 1 of Warren et al. (1999).

1.2.1 Low Interannual Variability in W99 Implementation

The W99 climatology is by definition invariant from year to year, and was implemented in this way by Laxon et al. (2003) and Giles et al. (2008a, b) to estimate sea ice thickness using the European Remote Sensing satellites 1 & 2. When implemented like this, the snow contribution term ($\overline{Snow}$) in Eq. (2) exhibits no interannual variability.

120   The implementation of W99 was then modified by Laxon et al. (2013) based on the results of Operation IceBridge flights which showed reduced snow depth over first year ice (FYI; Kurtz and Farrell, 2011). This implementation, known as 'mW99', consists of halving snow depths over first year ice with snow density kept constant. Because the areal fraction and spatial distribution of FYI changes from year to year, this modification introduces a small degree of interannual variability into the contribution of snow data to sea ice thickness.

125   But how does this variability compare with the true interannual variability of snow depth? Monthly values for the interannual variability in snow water equivalent and depth are given by Warren et al. (1999), but these are not currently used in sea ice thickness retrievals. Nonetheless, they offer a benchmark against which to evaluate interannual variability in mW99.

     The W99 monthly interannual variability (IAV) values are calculated as the standard deviation of the snow depths at drifting stations when compared to the climatology at the position of the stations. The IAV values at a drifting station in a region will

130 therefore naturally be higher than the IAV of the region's spatial-mean. As such, to compare IAV values from drifting stations to those created by the ice-type-based implementation of mW99, we calculate the IAV at all ice-covered points on a 25×25km equal-area grid (Brodzik et al., 2012) so as to simulate a drifting station at each point on the grid - we then average these IAV values. Using the ice age data described in Sect. 2.2, we find the variability introduced at a given point for mW99 was on average half of the value presented in W99 (Fig. 1). By comparison, SnowModel-LG snow depth variability (when calculated

135 in the same way) was significantly higher, ranging from ∼80% of the W99 value in October to ∼120% by the end of winter.
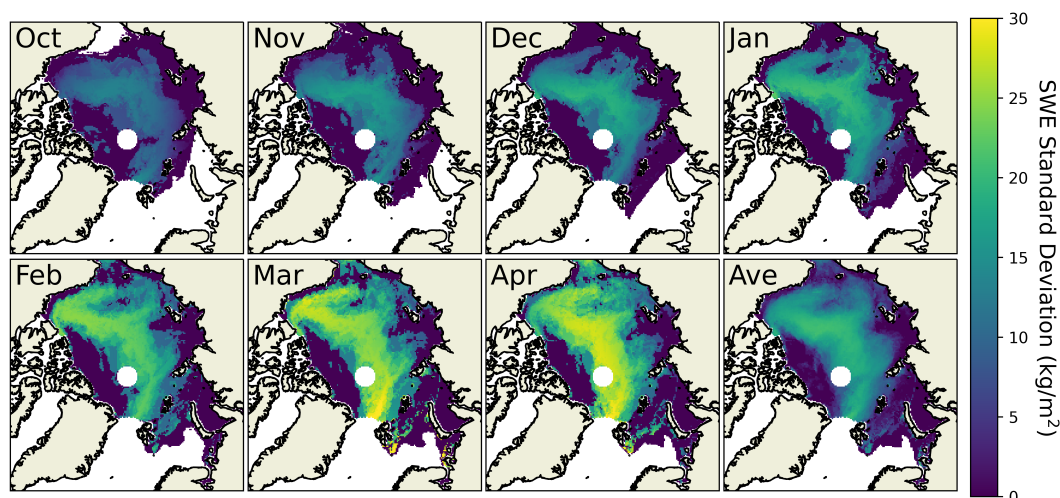
Figure 2. mW99 SWE variability at each grid point over the 2002-2018 period. Variability is displayed in a band where ice type typically fluctuates from year to year. IAV is zero in areas that do not exhibit ice-type variability, introducing unphysically low variability in SIT.

We present this result to illustrate that the conventional implementation of mW99 does not introduce enough variability at a given point to match that observed at drifting station locations from year to year. Furthermore, the variability that does exist is confined to a distinct band of the Arctic Ocean where the ice type typically varies from year to year (Fig. 2). In areas where ice type is temporally consistent, variability is not present. This has implications at the regional scale as marginal seas with a

140 consistent ice type experience unrealistically low $\sigma_{\overline{Snow}}$ in the mW99 scheme.

However, this paper does not focus on the interannual variability at a point (as measured by drifting stations and illustrated in Fig.1), but instead investigates the variability in $\overline{Snow}$ and $\overline{SIT}$ at the regional scale. This variability is significantly lower than the typical variability at a point, as many local anomalies from climatology within a region are smoothed out in the calculation of single, area-averaged annual values.

145 In this paper we calculate the three terms of Eq. (5): $\sigma^2_{\overline{Snow}}$ is calculated from mW99 and SnowModel-LG (Sect. 2.5) and $\sigma_{\overline{RF}}$ from radar freeboard data from the EnviSat and CryoSat-2 radar altimeters (Sect. 2.4). The covariance term is a function of both the preceding terms. We consider the relative contributions of these three terms to $\sigma^2_{\overline{SIT}}$ in calculations involving mW99 and SnowModel-LG (Sect. 4.1).

In light of these results, we then re-assess the statistical significance of regional trends in $\overline{SIT}$ using SnowModel-LG.

150 **1.2.2 Lack of Temporal Trends in W99 Implementation**

Weak trends exist in the mW99 Arctic snow distribution due to the shifting distribution and abundance of first year ice in the Arctic. In this section we briefly address their size, sign and veracity on a basin-wide scale, leaving regional analysis until Sect. (4.1).
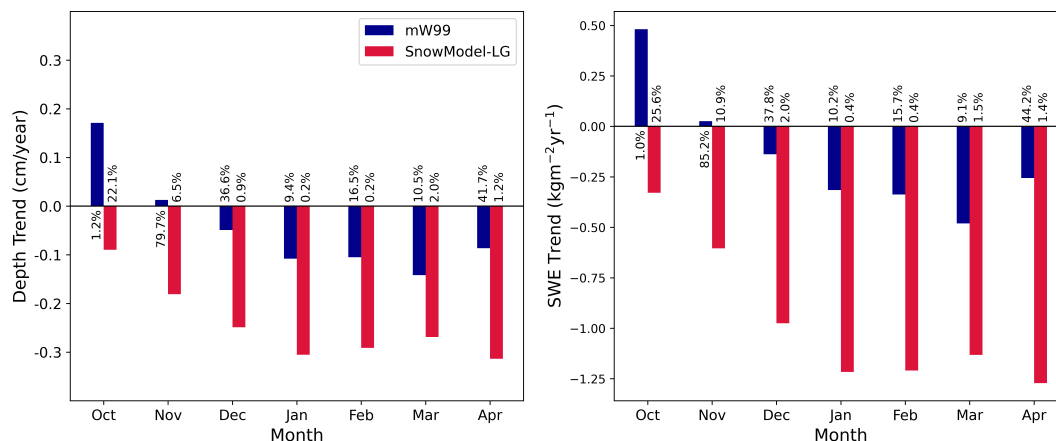
Figure 3. Trends in basin-wide mean (a) snow depth and (b) SWE, from mW99 and SnowModel-LG. Calculated for the Envisat-CS2 period (2002-2018). Significance values (in %) are given at the base of each bar. Only October trends for mW99 are significant at the 5% level, whereas significant negative trends exist in SnowModel-LG for December - April.

Values for SWE and depth trends measured by individual drifting stations are given in W99, but the values are not statistically

155   significant for any of the winter months considered in this paper, and as such are not displayed here. We instead compare the trends in basin-wide snow depth and SWE between mW99 and SnowModel-LG.

We find that the only statistically significant trend for mW99 snow depth is a positive one for the month of October (+0.18 cm/yr; Fig. 3). This increasing trend in snow depth is due to the diminishing area of October FYI relative to that of MYI (Fig. S2). This increasing October areal dominance of MYI is driven by delayed Arctic freeze-up (Markus et al., 2009; Stroeve et al.,

160   2014). The area of ice over which the W99 climatology is halved in October is therefore shrinking, and basin-wide mean snow depths in mW99 are increasing. Trends in ice-type fraction for each winter month are displayed in Fig. (S2), and monthly timeseries for mW99 SWE are displayed in Fig. (S3).

Unlike mW99, SnowModel-LG exhibits statistically significant, negative trends for the later five of the seven winter months at a basin-wide scale. Several processes are responsible for this decreasing trend: growth seasons now begin significantly

165   later, with a lower ice area exposed during the high snowfall months of September and October (Boisvert et al., 2018); also the later months of the Arctic winter are increasingly dominated by FYI, which cannot accumulate snow from year to year. Webster et al. (2014) observed a -0.29cm/yr trend in Western Arctic spring snow depths using a variety of *in situ* sources. This compares well with the behaviour of SnowModel-LG (-0.27 cm/yr March; -0.31 cm/yr April), but considerably beyond that of of the non-statistically significant trends of W99 and mW99.

170   How might the reality of decreasing SWE affect satellite derived estimations of $\overline{SIT}$? Under the paradigm of total radar wave penetration of snow on sea ice, under-accounting for potential reductions in SWE may partially mask a decline in sea ice

thickness, as reductions in radar freeboards are partially compensated by reductions in snow depths.

$$\frac{\partial(\overline{SIT})}{\partial t} = \frac{\partial(\overline{RF})}{\partial t} + \frac{\partial(\overline{Snow})}{\partial t} \tag{6}$$

Put another way, models and observations indicate that $\partial(\overline{Snow})/\partial t$ is negative on long timescales (Webster et al., 2014; Warren et al., 1999; Stroeve et al., 2020). However, the use of mW99 sets $\partial(\overline{Snow})/\partial t$ to zero, and to a positive value in October. This has the effect of biasing $\partial(\overline{SIT})/\partial t$ high (and towards zero). Section 4.2 examines the effect of using SWE data with a more realistic decline on $\overline{SIT}$ trends; this is mediated by the effects of higher interannual variability, introduced in Sect. (4.1).

2   Data Description

2.1   Regional Mask

We define six regions of the Arctic Basin using the mask from Stroeve et al. (2014) which is gridded onto a 25 km resolution EASE grid (Brodzik et al., 2012, Fig. 4). We define the 'marginal seas' of the Arctic Basin as the shaded areas of Fig. (4) excluding the Central Arctic. All constituent regions of the 'marginal seas' grouping lie within the coverage of Envisat barring a negligible portion of the Laptev Sea.

2.2   Ice Type Data

Sea ice type data was required to modify W99 and create mW99. To do this we used the sea ice type product of the EUMETSAT Ocean and Sea Ice Satellite Application Facility (OSI SAF, www.osi-saf.org). This data series begins in 2005. Where sea ice type was required prior to 2005 for Envisat retrievals, we used data from the Copernicus climate data record from satellite sensors (CDS, www.cds.climate.copernicus.eu).

2.3   W99

The Warren Climatology includes quadratic fits for every month of snow water equivalent and snow depth. We projected these fits over the 361×361 EASE grid (for comparison with SnowModel-LG) to create SWE and depth distributions across the Arctic basin as defined in Sect. (2.1). Where our ice type data indicated first year ice, W99 depth and SWE was halved as per Laxon et al. (2013).

In some months the ice type for a pixel was ambiguous: in the case where the pixel was surrounded by a given ice type we interpolated the value. In the case where the pixel existed on the FYI/MYI boundary, the snow depth was not divided by two. These cases were relatively rare and thus are not anticipated to bias the results to a significant degree.
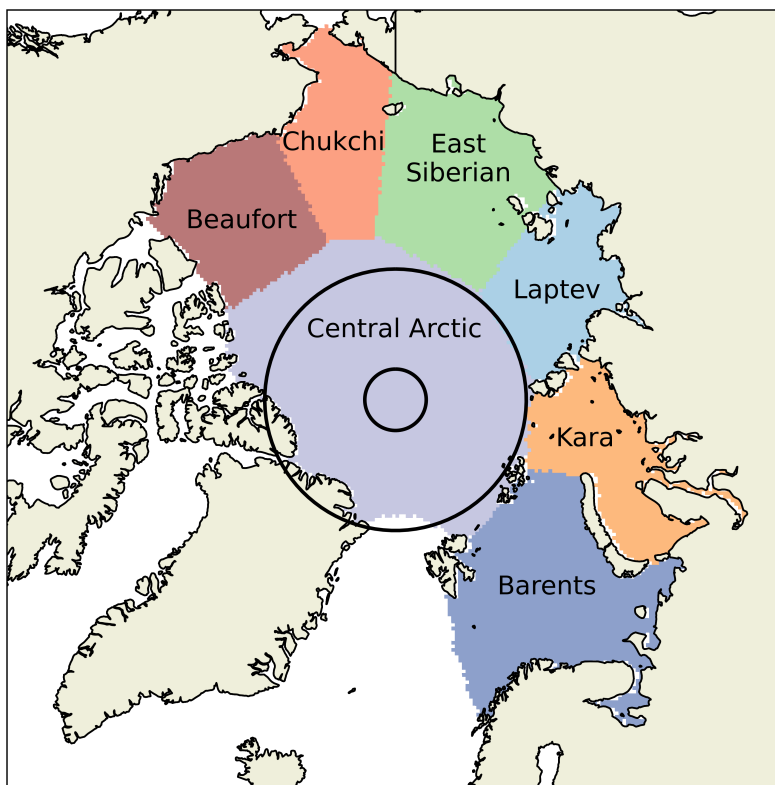
Figure 4. The definitions of the marginal Arctic seas used in this paper, from Stroeve et al. (2014). Two black, concentric circles indicate the latitudinal limits of the CryoSat-2 (inner circle; 88°N) and Envisat (outer circle; 82.5°N) missions.

2.4 Radar Freeboard Data

To examine the impact of snow products on Enivsat/CryoSat-2 thickness retrievals, we used radar freeboard data from the ESA
200 Sea Ice Climate Change Initiative (Hendricks et al., 2018). This product was chosen for two main reasons: (a) it provides a consistent record for both the Envisat and CS2 missions (Paul et al., 2018), and (b) it is publicly available for download. This data is supplied on a Lambert Azimuthal Equal Area grid and was regridded to the 25km EASE grid prior to analysis.

2.5 SnowModel-LG

To investigate variability and trends in $\overline{SIT}$ we use the results of SnowModel-LG (Liston et al., 2020; Stroeve et al., 2020).
205 SnowModel-LG is a Lagrangian model for snow accumulation over sea ice; the model assimilates reanalysis weather data and combines them with ice motion vectors to generate pan-Arctic snow depth and density distributions. SnowModel-LG exhibits more significant interannual variability than mW99 in its output because it reflects year to year variations in weather and ice dynamics.

SnowModel-LG includes a relatively advanced degree of physics in its modelling of winter snow accumulation. Snow

210 sublimation, wind-packing and snow-ice accumulation are included. However, the effects of loss of snow to leads by wind and extra snow accumulation due to ice roughness are not included. Furthermore, the heat flux to the snow is not sensitive to the thickness of the underlying ice.

SnowModel-LG creates a snow distribution based on reanalysis data, and the accuracy of this snow data is unlikely to exceed the accuracy of the input. There is significant spread in the results of reanalysis over the Arctic ocean (Barrett et al., 2020), and

215 the results of SnowModel-LG depend on the reanalysis data set used. However, the data product used has been tuned to match Operation Ice Bridge derived snow depths during spring time, and snow depth differences between the reanalysis products were found to be less than 5 cm (Stroeve et al., 2020). The data used in this study are generated from the average of SnowModel-LG runs forced by the MERRA-2 and ERA-5 reanalysis products.

2.6 NASA Eulerian Snow on Sea Ice Model (NESOSIM)

220 To support and broaden the impact of our findings, we repeat our analyses with NESOSIM data from 2002-2015 (Petty et al., 2018b). NESOSIM data is released on a 100×100 km grid which was interpolated to the 25×25km EASE grid of SnowModel-LG data. NESOSIM runs in a Eulerian framework and like SnowModel-LG can be driven by a variety of reanalyses. It uses a two-layer snow scheme representing depth-hoar and wind-packed layers. To define these layers, it assimilates surface winds and temperature profiles from reanalysis. The snow pack is initialised using values from W99 and parameterises wind-blown

225 loss to leads using daily sea ice concentration fields (Comiso, 2000, updated 2017).

3 Methods

3.1 Interannual Variability

In Sect. (4.1) we calculate the covariance matrix of the two terms of Eq. (2) for each region in each month. The three unique components of the 2×2 covariance matrix are the terms of Eq. (5) and allow the calculation of interannual variability for the

230 region and time period under consideration.

The main-diagonal elements of this 2×2 matrix correspond to the variance of the snow contribution and the radar freeboard contribution to sea ice thickness, terms one and two of Eq. (5). The off-diagonal elements are identical and sum to form the third term of Eq. (5).

In some cases a natural degree of covariance is introduced between the regional $\overline{Snow}$ and $\overline{RF}$ timeseries because they both

235 display a decreasing trend. This 'false-variance' would not be present were the system in a steady state. As such, we detrended the regional timeseries prior to calculation of the covariance matrix. We found that doing this significantly decreased the value of the covariance term in Eq. (5) .

The Central Arctic region exists above the latitudinal limit of the Envisat orbit, so the covariance matrix for the region was only calculated for the CS2 period (2010-2018).

3.2 Temporal Trends

In Sect (4.2) we examine temporal trends in regional $\overline{SIT}$ for each month of the growth-season (October - April), and decompose the results by ice type. It is stressed that this is the trend of a single timeseries of average thickness values, rather than the average of several trends in sea ice thickness at various pixels in a region. Regional trends were deemed statistically significant if they passed a two-tailed Wald test with p-value less than 0.05, with a null hypothesis of no trend. Trends were calculated for regional $\overline{SIT}$ over the Envisat-CS2 period (2002-2018) for all regions apart from the Central Arctic for which only CS2 data was available.

4 Results

4.1 Realistic SWE Interannual Variability Enhances SIT Interannual Variability

We first analysed the variability of detrended timeseries of $\overline{Snow}$ from mW99 and SnowModel-LG. We did this for every winter month (Oct-Apr) and in each region defined in Fig. (4). SnowModel-LG data produce more variable timeseries of $\overline{Snow}$ (i.e. higher values of $\sigma^2_{\overline{Snow}}$; c.f. Eq. 5). This is the case for all months, in all regions (Fig. 5). This is sometimes the case by several orders of magnitude: for snow in the Kara Sea, mW99 introduces almost no interannual variability into SIT via $\overline{Snow}$, whereas SnowModel-LG introduces 0.26 m of thickness variability to the April timeseries. This analysis is further broken down by ice type in Figs S4 and S5.

Having shown that SnowModel's contribution to sea ice thickness is more variable than mW99, how does this increased variability propagate into sea ice thickness variability itself ($\sigma^2_{\overline{SIT}}$)? To answer this question, we examine the way in which the snow contribution to SIT combines with data from satellite radar freeboard measurements. Having calculated the $\sigma^2_{\overline{Snow}}$ term of Eq. 5, we now turn to the $2\,\mathrm{Cov}(\overline{RF}, \overline{Snow})$ term. To assess this we calculate the magnitude and statistical significance of correlations between the $\overline{RF}$ and $\overline{Snow}$ contributions to $\overline{SIT}$ in individual years, regions and months.

We find statistically significant correlations between $\overline{Snow}$ and $\overline{RF}$ to generally range between 0.5 - 0.7 (Fig. 6). All statistically significant correlations were positive ones, and this was also the case when individual ice types were considered for each region. When all ice types were considered, the Laptev and East Siberian seas exhibited statistically significant trends in five of the seven growth-season months. The Barents Sea and the Central Arctic Region both exhibited no months of correlation. When analysed as a single, large region, the 'Marginal Seas' area exhibits correlations in four of the seven months analysed.

We continued this analysis by breaking down the regions by ice type. The area of the Central Arctic sea ice covered with first year ice exhibits strong correlations (in the range 0.74 - 0.96) in the months of October, January, February, March and April (Fig. S6). This analysis also introduced two months of correlation in the Barents Sea, which like the Central Arctic did not previously exhibit any.
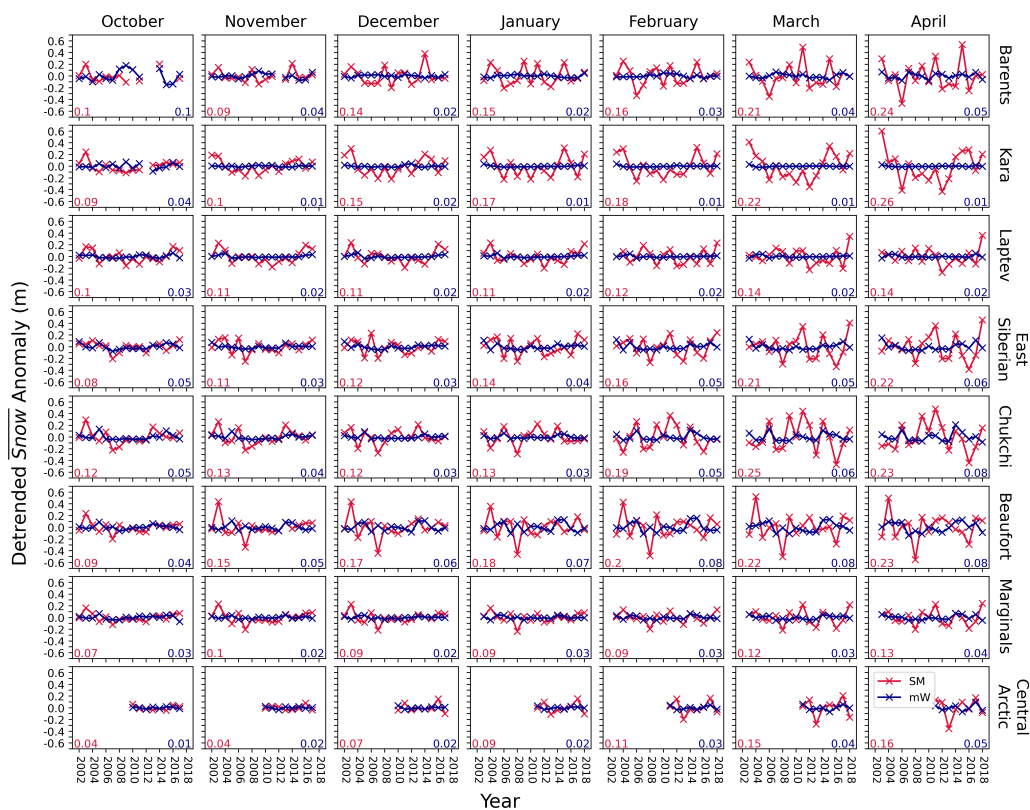
Figure 5. Detrended timeseries of spatially averaged snow contributions to sea ice thickness ($\overline{Snow}$) by region from W99 (blue) and SnowModel-LG (red). Standard deviation values are displayed for SnowModel-LG (lower left, red), and mW99 (lower right, blue).

When considering correlations over multi-year ice, the Laptev and East Siberian seas mirrored their 'all types' behaviour, this time exhibiting trends in four of the growth-season months (Fig. S7). In a further similarity to the 'all types' analysis, the Central Arctic exhibits no correlations.

We note that this analysis is relatively sensitive to the detrending process. When performed without detrending, statistically significant correlations are noticeably more common. This is because $\overline{Snow}$ and $\overline{RF}$ are both in decline in some areas, which introduces an inherent correlation from the trend.

Having identified and quantified regions and months of significant covariance between $\overline{Snow}$ and $\overline{RF}$ (Fig. 6), we are in a position to fully answer the question of how the increased variability of SnowModel-LG over mW99 (shown in Fig. 5) ultimately impacts $\sigma^2_{\overline{SIT}}$. We plot the three contributing components to $\sigma^2_{\overline{SIT}}$ in for each region in each winter month (Fig. 7).

In the marginal seas $\sigma^2_{\overline{Snow}}$ overtakes $\sigma^2_{\overline{RF}}$ to become the main constituent of $\sigma^2_{\overline{SIT}}$ by end of the growth season (Fig. 7). This is particularly the case in the Beaufort and Barents Seas, where an inverse relationship is clearly visible. In the Central Arctic $\sigma^2_{\overline{RF}}$ remains the dominant component of $\sigma^2_{\overline{SIT}}$, throughout the cold season although $\sigma^2_{\overline{Snow}}$ plays an increasing role
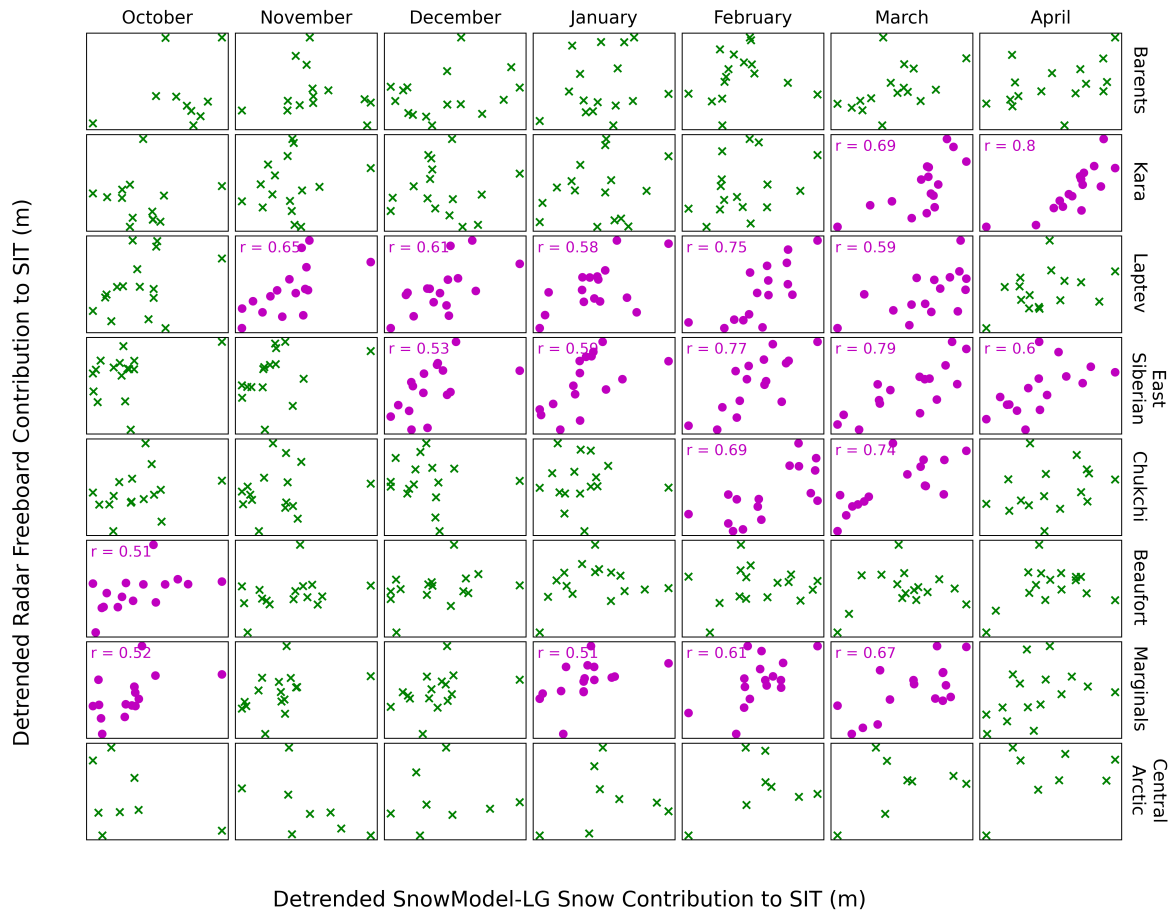
Figure 6. Covariability of contributions to sea ice thickness from radar freeboard and SnowModel-LG derived snow components over all ice types. Plots are colored with magenta when a a statistically significant correlation is present between the contributions (p>0.95). Analogous plots are displayed for the FYI and MYI components of the regions in Figs S6 & S7.

as the season progresses. We also analysed the marginal seas as a contiguous group; this gave rise to lower IAV values due to the averaging of spatial anomalies. However, the pattern of transition of dominance from $\sigma^2_{\overline{Snow}}$ to $\sigma^2_{\overline{RF}}$ remains a persistent feature.

285   Covariance between $\overline{RF}$ and $\overline{Snow}$ makes relatively constant contributions to $\sigma^2_{\overline{SIT}}$ of the 'marginal seas' grouping by comparison to the other two components, but analysis at this scale conceals more significant variation at that of the constituent regions. The covariability term of Eq. 5 makes a larger contribution than freeboard variability itself at times, for example in the Kara and East Siberian seas at the end-of-winter, and for the Chukchi Sea in February and March. For the Central Arctic, freeboard-snow covariability generally makes less of a contribution to total SIT variability than freeboard or snow variability

290   individually.
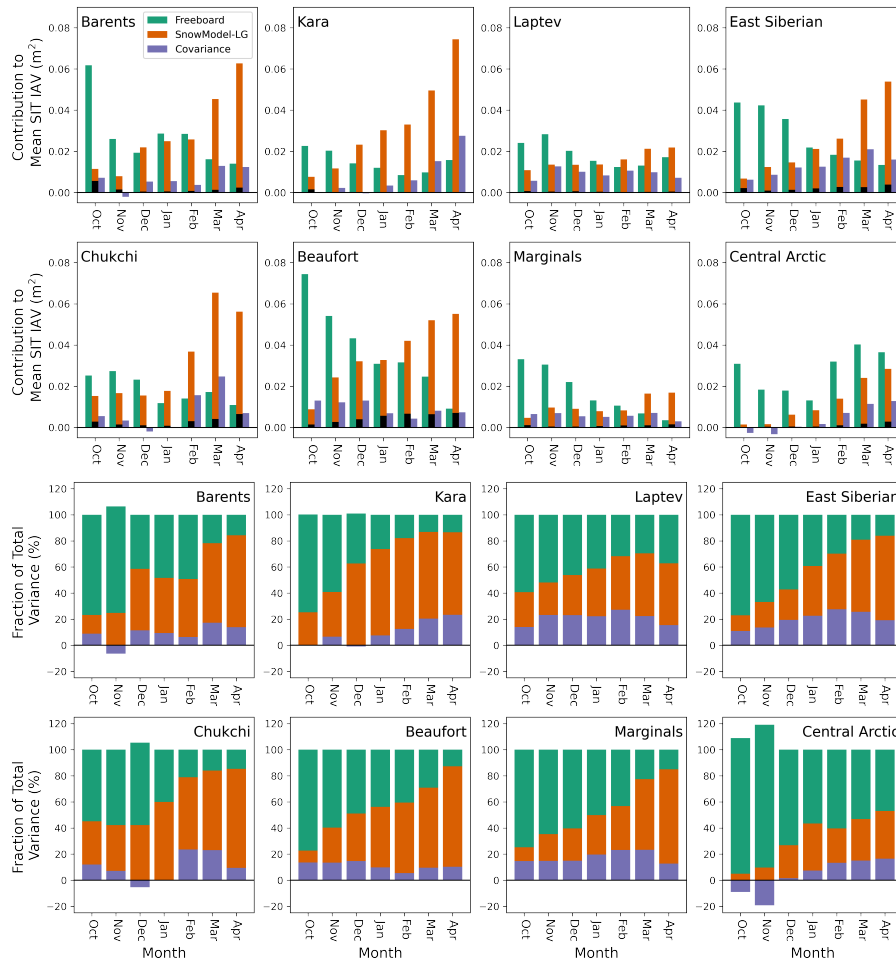
Figure 7. Constituent parts of $\sigma^2_{\overline{SIT}}$ of different regions. Bars represent the variance (σ^2) of $\overline{RF}$ and $\overline{Snow}$ and the covariance between the two. (a) illustrates the absolute variance contributions (b) illustrates their relative contributions. The variance of $\overline{Snow}$ in mW99 is indicated in figure (a) by a superimposed black bar. Snow contributes significantly more variability in the late winter than radar freeboard in most of the marginal seas.

Finally, we directly compare the variability of $\overline{SIT}$ itself, when calculated using SnowModel-LG and mW99. We conduct this exercise in both absolute terms (Fig. 8a) and as a fraction of the regional mean thickness (Fig. 8b).

Calculation with SnowModel-LG reveals higher variability in all marginal seas of the Arctic basin in all months. When the marginal seas are analysed as a continuous entity, the standard deviation is 0.12 m with mW99 and 0.19 m with SnowModel-

295 LG. This represents an increase in $\overline{SIT}$ variability of 58%. For the Central Arctic this figure is considerably smaller, at 27%. When the individual marginal seas are considered, the largest increase was the Kara Sea (121%) and the smallest was in the Beaufort Sea (41%).

One key aspect of interannual variability is how it compares to typical values. When IAV is expressed as a percentage of the regional mean thickness, the Barents Sea exhibits the largest increase when calculated with SnowModel-LG: the standard

300 deviation (as a percentage of mean thickness) increases from 14% to 24%. When variability is viewed in this way, the increase in the Central Arctic is small (7.1% to 8.6%). Variability as a fraction of mean thickness is also highest in the Barents Sea when calculated with SnowModel-LG - whereas with mW99 this designation would go to the Beaufort Sea. When analysed as one area, variability (as a fraction of mean thickness) in the marginal seas transitions from being 10.4% of the mean thickness to 16.6%.

305 We also note that MYI exhibits more thickness variability than FYI (both absolutely and relative to the ice type's mean thickness) in all the marginal seas (Fig. S8). For the marginal seas as a single group, MYI is roughly twice as variable (in both absolute and relative senses). This is not the case in the Central Arctic, where the thickness variability of the individual ice types is almost exactly the same (with FYI IAV slightly larger when calculated relative to regional mean thickness).
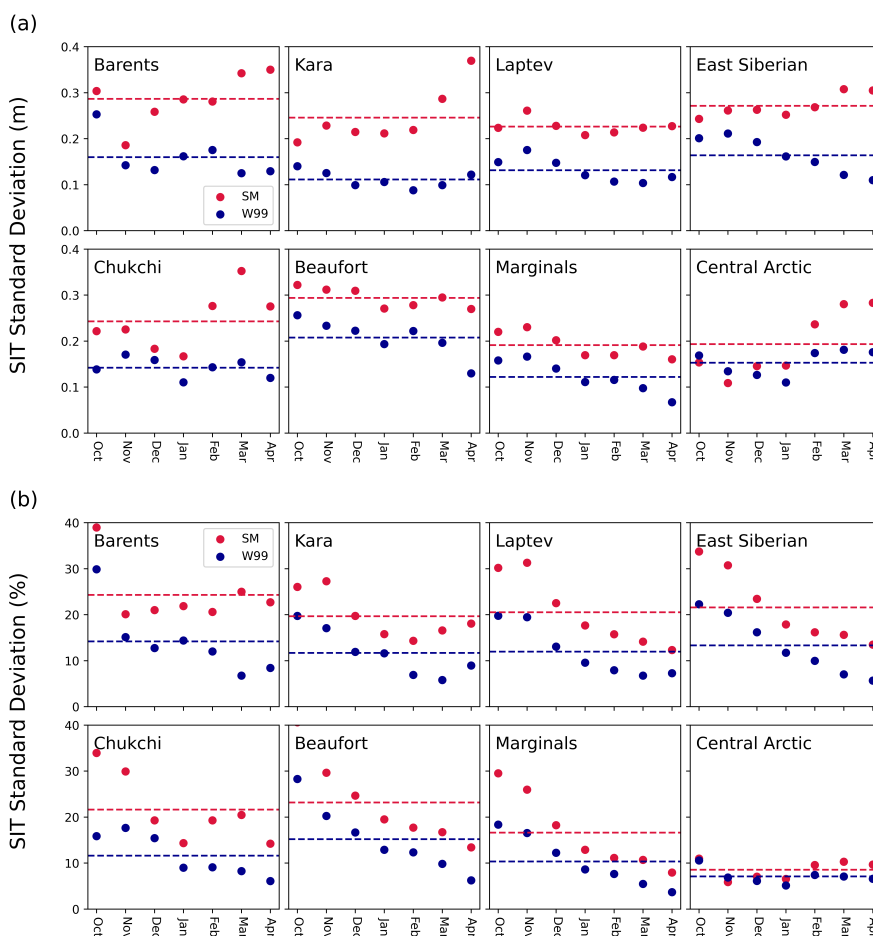
Figure 8. Standard deviation in sea ice thickness over the period 2002 - 2018. (a) calculated in absolute terms (b) calculated as a percentage of the regional mean thickness over the period. Mean growth-season values shown with dashed lines. The individual detrended regional timeseries from which this figure is synthesised are available in Fig. S9.

4.2 New and faster thickness declines in the marginal seas

As well as exhibiting higher interannual variability than mW99, SnowModel-LG $\overline{Snow}$ values decline over time in most regions due to decreasing SWE values year-on-year. Here we examine the aggregate contribution of a more variable but declining $\overline{Snow}$ timeseries in determining the magnitude and significance of trends in $\overline{SIT}$.

We first assess regions where $\overline{SIT}$ was already in statistically significant decline when calculated with mW99. This is the case for all months in the Barents and Kara seas, and six of seven months in the Laptev sea. The rate of decline in these regions significantly increased when calculated with SnowModel-LG data (Fig. 9). Relative to the decline-rate calculated with mW99, this represents average increases of 70% in the Laptev sea, 98% in the Kara Sea, and 106% in the Barents Sea. In the Chukchi

Sea, where three of the seven months exhibited statistically significant decline with mW99 data, those three months exhibited on average a 98% faster decline. The largest increase in an already statistically-significant decline was in the Chukchi Sea in April, where the decline-rate increased from 1.5 cm/yr to 3.9 cm/yr, an increase of 173% or a factor of 2.6. When analysed

320 as an aggregated area and with mW99, the total 'Marginal Seas' area exhibits a statistically significant declining trend in the last month of the growth season: April. When calculated with SnowModel-LG data, the magnitude of this trend is more than doubled (from 1.6 cm/yr to 3.5 cm/yr, 118% increase). This increased trend is largely driven by thicker ice in years prior to 2012, with the exception of 2008.

We now turn our attention to new trends, induced by the use of SnowModel-LG over mW99. Our analysis reveals a new,

325 statistically significant $\overline{SIT}$ decline in the Chukchi Sea in November (taking the number of declining months to four). This is driven by the sea ice being thinner after 2006, with values being more similar to mW99 in the years prior to 2006. Perhaps more significantly, the aggregated Marginal Seas region exhibits three new months of statistically significant declining $\overline{SIT}$ in December, January and February. This new significance is largely driven by thicker ice in 2003 and 2004. No months in any marginal sea exhibited a statistically significant increasing trend in $\overline{SIT}$ (with either snow data set).

330 For the first two months of the growth season (October and November), the Central Arctic region exhibits a statistically significant thickening trend with both snow data sets (10 cm/yr and 6 cm/yr for Oct and Nov with mW99). In these months the use of SnowModel-LG increases this growth by 1 and 2 cm/yr. The subsequent two months (December and January) are only ones of statistically significant thickening when calculated with mW99 (6 cm/yr and 5 cm/yr); when calculated with SnowModel-LG they do not show a statistically significant trend.

335 We also analyse these regional declines as a percentage of the regional mean ice thickness in the observational period (2002-2018). We observe the average growth-season thinning to increase from 21% per decade to 45% per decade in the Barents Sea, 31% to 50% per decade in the Kara Sea, and 20% to 36% per decade in the Laptev Sea. Four of the seven growth-season months in the Chukchi Sea exhibit a decline with SnowModel-LG of (on average) 34% per decade. This is more than double that of the three significant months observable with mW99 (15% per decade). We find the Marginal Seas (when considered as

340 a contiguous, aggregated group) to be losing 20% of its mean thickness per decade in the four statistically significant months.

We further analyse these declining trends by ice-type. This reveals the aggregate trends in the marginal seas to be broadly driven by thickness decline in FYI, as the MYI component is only in decline for April. Barents Sea FYI thickness is in statistically significant decline (independent of ice type) in six of the seven growth-season months, whereas Barents Sea MYI thickness snows no trend for any month. Just as the Beaufort and East Siberian Seas snow no trend for an all-ice-type analysis,

345 neither their FYI or MYI components show trends in any growth-season month. We find that (when analysed with SnowModel-LG) if any month in a specific marginal sea is in 'all types' decline, its FYI ice is also statistically significantly declining.

4.3 Changes to the sea ice thickness distribution and seasonal growth

We now consider differences in the spatial sea ice thickness distribution introduced by a snow product with IAV. Because mW99 has low spatial variability in its SWE fields (the quadratic fits are relatively flat), it produces a more sharply peaked and

350 truncated SIT distribution with lower probabilities of thinner or thicker ice. The SIT distribution also exhibits some degree of
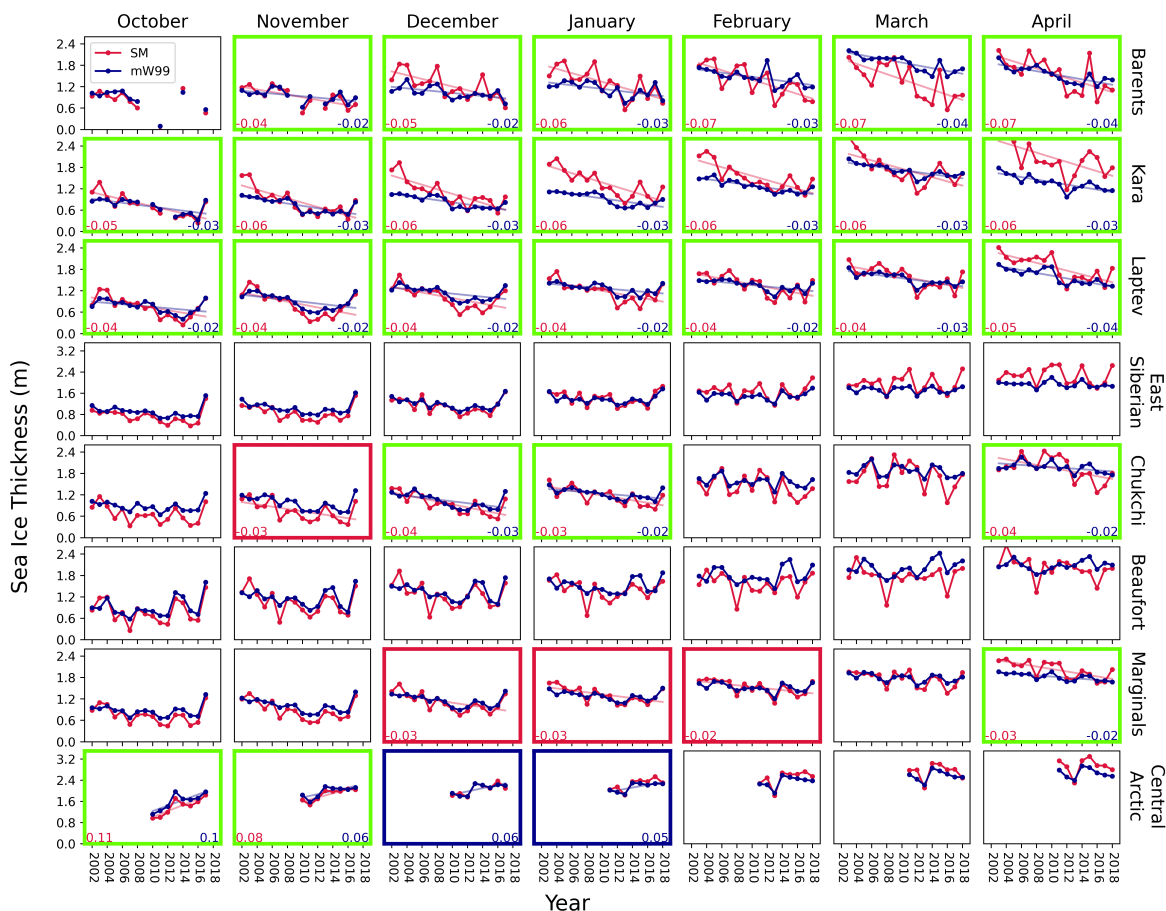
Figure 9. Regional $\overline{SIT}$ timeseries calculated using mW99 and SnowModel-LG. Panels featuring a statistically significant trend in sea ice thickness when calculated both mW99 & SnowModel-LG framed with green. Red frames indicate where trend is only significant when calculated with SnowModel-LG. Blue frames indicate where a statistically significant increase is detected with mW99, but not with SnowModel-LG. Where trends are statistically significant, trend lines are superimposed. Positive trends exist for the first four months of the Central Arctic, although only October is significant for both mW99 and SnowModel-LG calculations.
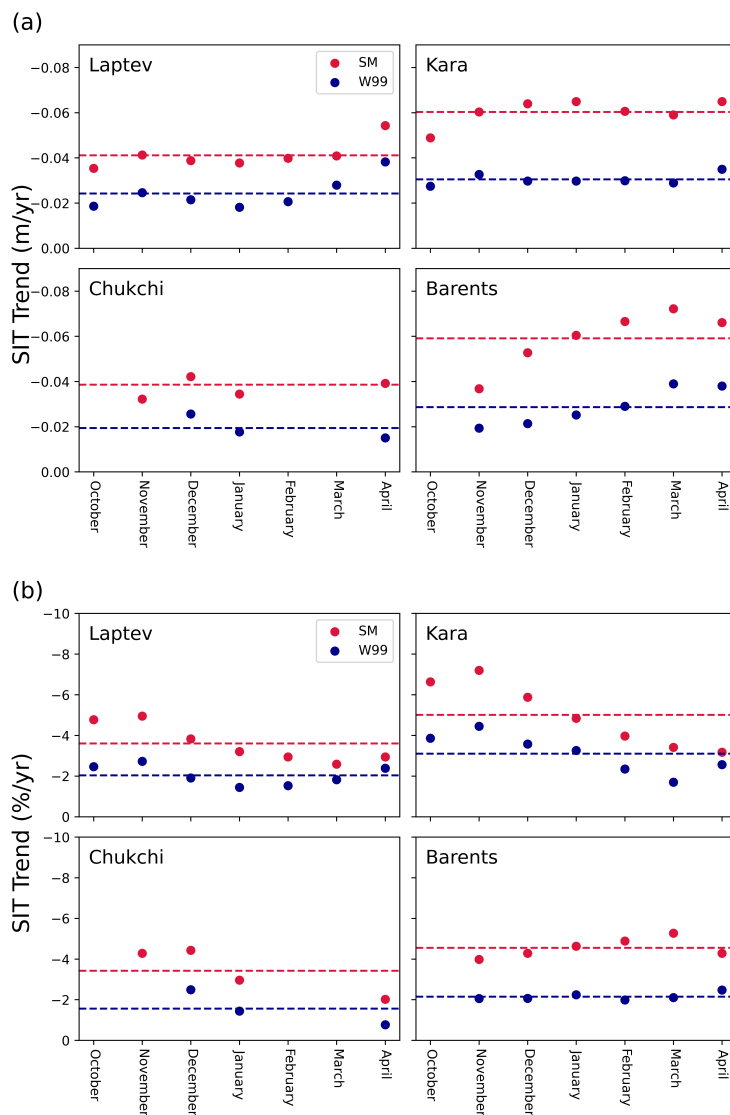
Figure 10. Sea ice thickness trends in the four marginal seas that exhibited robust trends in several winter months in the period 2002-2018. Average winter trend (calculated only from statistically significant months) from each snow product shown with dashed lines. Data points are only shown where a statistically significant trend is present for that month and for the relevant snow data.

bimodality due to the halving scheme. This bimodality is to a large degree represented in the SnowModel-LG histograms - an encouraging result (Fig. S10).

The regional, seasonal growth rate is also similar when comparing calculations with SnowModel-LG and mW99 (Fig. S11). Among the most salient differences are the decline in SWE from March to April in the Barents and Kara Sea with mW99 (compared to a continued increase with SnowModel-LG), and the roughly equal SIT distribution for March and April for the

355

aggregated Marginal Seas area. In the East Siberian there is clearly a slightly lower seasonal growth rate when calculated with mW99, and this is also true for the Chukchi Sea.

5 Discussion

5.1 Sensitivity of Findings to Choice of Snow Product

360 #### 5.1.1 Choice of Climatology - Combining AMSR2 with mW99

The most recent sea ice thickness product from the Alfred Wegener Institute (Hendricks and Ricker, 2019) makes use of a new snow climatology, generated by the merging of W99 with snow depth data derived from the AMSR2 passive microwave record. This is then applied with a halving scheme based on ice-type in a similar way to mW99 (but with the AMSR2 component not halved). This likely improves the absolute accuracy of snow depths (and thus sea ice thickness), but does not resolve the issues

365 discussed in this paper involving trends and variability. The modified AMSR2/W99 functions in a very similar way to mW99 - a weak IAV is introduced in areas of interannually fluctuating ice type. Any trends will be the result of trends in the relative dominance of ice-type. This was discussed in Sect. 1.2.2 and illustrated in Fig. S2: ice type trends are only significant in October and January, where they are weak.

5.1.2 Choice of Reanalysis Forcing for SnowModel-LG

370 Barrett et al. (2020) reviewed precipitation data from various reanalysis products over the Arctic Ocean, and found the magnitude of interannual variability to be similar. They further broke these data down to the regional scale using the same regional definitions in this paper, and found that this similarity persisted. To investigate how this variability propagates into $\overline{Snow}$ variability, we calculate $\overline{Snow}$ timeseries from SnowModel-LG runs forced by both MERRA-2 and ERA-5 data and find their variances to be very similar (Fig. S12).

375 With regard to trends, we find that the two different reanalysis forcings generally introduce minimal differences in the SIT trends (Fig. S13). We do however find that small differences in SWE cause the $\overline{Snow}$ contribution of the MERRA-2 SnowModel-LG run to exhibit statistically signfcant decline in regions and months where the ERA-5 run does not (with only a small change to the p-value). Analysis of the absolute $\overline{Snow}$ timeseries reveals them to be otherwise similar (Fig. S14).

We take these clear similarities as evidence that our findings are in principle robust to the choice of atmospheric reanalysis.

380 #### 5.1.3 Choice of Model - Comparison with NESOSIM

Some uncertainty is introduced into the spatial distribution of snow in a given year by SnowModel-LG snow parameterisations and simplifications, such as the lack of snow loss to leads. We therefore repeat our analyses with 2002-2015 data from the NASA Eulerian Snow On Sea Ice Model (NESOSIM; Petty et al., 2018b).

We find that doing this increases the relative importance of snow variability to sea ice thickness variability (Fig. S15). We

385 also observe that the NESOSIM calculations are considerably more similar to those done with SnowModel-LG than with

mW99. NESOSIM replicates the increasingly dominant $\sigma^2_{\overline{Snow}}$ contribution to $\sigma^2_{\overline{SIT}}$ over the winter in the Marginal seas, and also replicates the higher contribution of $\sigma^2_{\overline{RF}}$ in the Central Arctic compared to both the individual and aggregated marginal seas. Striking resemblances are seen for the Kara Sea and the East Siberian Sea. Furthermore, the negative covariance for November in the Barents Sea is replicated, as well as those in the Central Arctic in November and December.

390   Because the NESOSIM data is only publicly available from 2002-2015, any underlying trends in the SIT timeseries are more challenging to detect because of the truncated observational period. On the other hand, the calculated interannual variability is not reduced by truncation of the timeseries, further obscuring any potential underlying trends. However, we find that the radar freeboards in the winter of 2017-2018 were anomalously high in the Marginal Seas (c.f. Fig. 9), creating a 'trend-bucking' year. As such, despite its shorter span, the 'NESOSIM period' exhibits more trends than the 'SnowModel-LG period' by

395   excluding this anomalous winter (Fig. 11). For example in this period (2002-2015), six of the seven growth-season months in the aggregated Marginal Seas area exhibit declining trends when calculated with SnowModel-LG (compared to four when calculated over the full 2002-2018 period). This is also evident in the East Siberian Sea, where the early growth-season months of October, November and December all exhibit statistically significant decline when calculated with either NESOSIM or SnowModel-LG when assessed over 2002-2015 (but exhibit no trend over 2002-2018).

400   However we choose not to focus further on the steeper and more abundant absolute trend results in this shorter period, as the three winters of 2015-2018 cannot be ignored for statistical convenience. We instead use this time period to assess differences in regional trends when mean sea ice thickness is calculated with SnowModel-LG and NESOSIM, in order to assess the robustness of our broader approach with SnowModel-LG. Binary trend significances (or lack thereof) are identical in the Laptev, East Siberian and Beaufort seas. They are near-identical in the Kara and Chukchi, where both regions have

405   one month of the year where a trend exists when calculated with SnowModel-LG but not with NESOSIM (Fig. 11). Further inspection of the individual datapoints across all regions and months reveals good agreement in SIT when calculated with either SnowModel-LG or NESOSIM - we take this as evidence that our findings concerning trends and variability over the longer 2002-2018 period are robust to the choice of reanalysis-accumulation model.
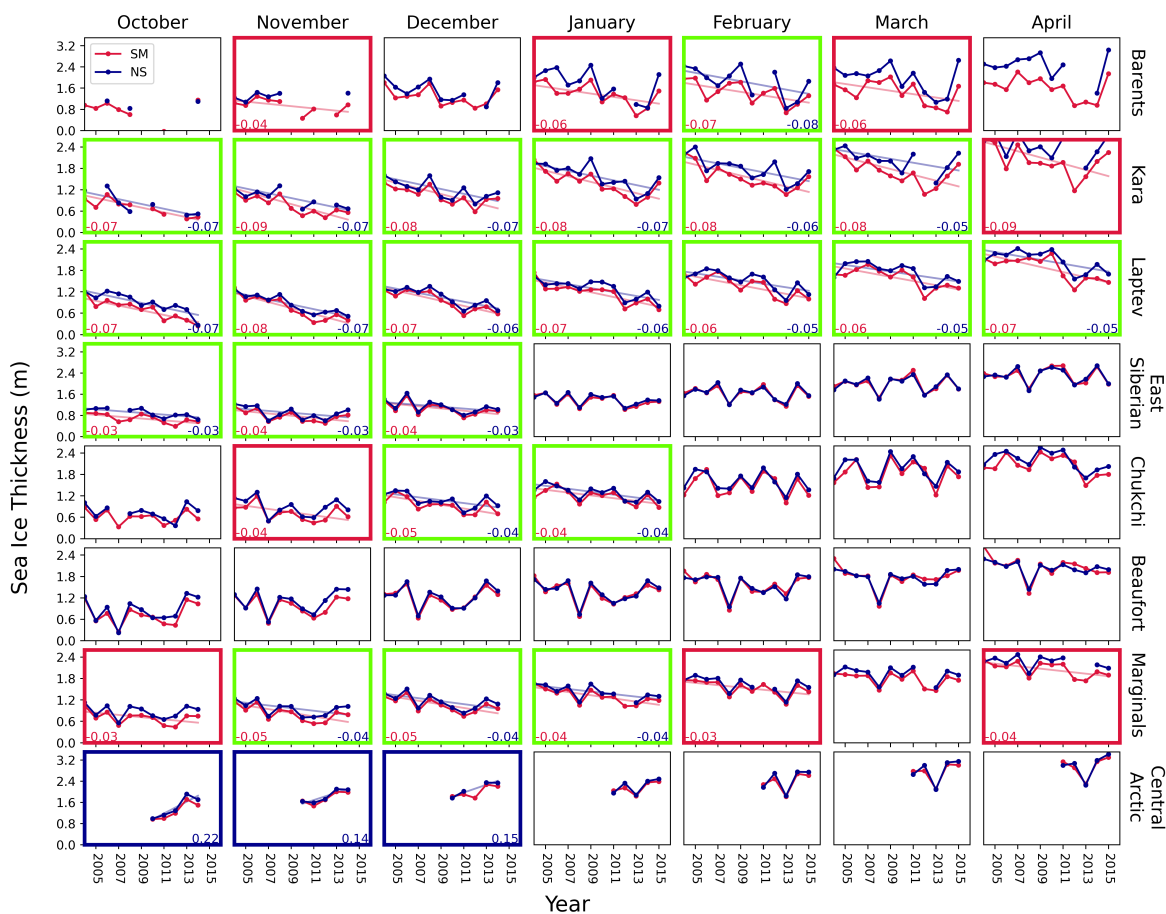
Figure 11. Regional $\overline{SIT}$ timeseries calculated using SnowModel-LG (red) and NESOSIM (blue). For the purposes of inter-product comparison, data shown (and trends calculated) are for the period 2002-2015 (a period shorter than previously analysed). Panels featuring a statistically significant trend in sea ice thickness when calculated both SnowModel-LG & NESOSIM framed with green. Red frames indicate where trend is only significant when calculated with SnowModel-LG. Blue frames indicate where a statistically significant increase is detected with NESOSIM, but not with SnowModel-LG. Where trends are statistically significant, trend lines are superimposed. SIT data is highly similar when calculated with either snow data set, indicating that our broader findings are robust to our choice of reanalysis-accumulation model.

5.2 Study Limitations

410   5.2.1   Statistical Treatment

We have assumed in calculating single figures for variances that the interannual variability of the systems at hand is time-stationary. It is unclear whether this is the case, as the timeseries are limited in length and time-resolution and thus offer limited scope to test for stationarity. Furthermore we only tested for linear trends, when trends may in fact be non-linear. However, a visual inspection of Fig. (9) implies that this approximation is adequate on a qualitative level. Our trend tests also were two-

415 tailed, with the null hypothesis that there was no trend. We could have formulated an alternate test where our null hypothesis was that the trend was positive. This would have given a higher number of statistically significant instances of negative trends, but we deemed this inappropriate as one of the regions (the Central Arctic) does exhibit significant positive trends with the two-tailed test.

5.2.2   The Effects of Incomplete Radar Penetration of the Snowpack

420 This investigation has been carried out within the paradigm of total Ku-band radar wave penetration of the snow cover (as suggested by Beaven et al. (1995)), however some in situ investigations have cast doubt on this. The issue was highlighted in an Antarctic context by Giles et al. (2008b) for ERS radar freeboards, and it was shown subsequently that significant morphological features in the snowpack (e.g. depth hoar, wet snow or crusts) enhanced radar scattering from within the snowpack (Willatt et al., 2010). For the Arctic, Willatt et al. (2011) found that airborne Ku-band radar backscatter in the Bay of Both-

425 nia was returned from nearer the snow-ice than snow-air interface in only 25% of cases when the temperature was close to freezing, the figure increasing to 80% at lower temperatures. Nandan et al. (2017) observed that the presence of brine in the base of the snowpack can raise the scattering horizon by several centimeters. However, these investigations were carried out at the end of the winter season or in the Sub-Arctic, when warmer temperatures increase the snow's brine volume fraction and diurnal forcing can drive rapid snow metamorphism. Both of these factors will be less prevalent in the colder months of winter.

430 This analysis is therefore carried out using the historical assumption present in publicly available sea ice products (that of total penetration).

What would the effects of incomplete penetration of the snowpack be on our findings? As the height of the primary radar scattering horizon rises through the snow, the altimeter operation transitions from that of a radar altimeter to that of a lidar altimeter. Knowledge of overlying snow contributes positively to the inference of SIT in the case of a radar altimeter (i.e. the

435 coefficient of m_s term of Eq. 2 is positive). However, the influence of overlying snow on lidar-based SIT estimates is negative (i.e. the presence of more snow for a given measured freeboard implies less underlying ice). As the scattering horizon rises through the snowpack, the SIT contribution of snow therefore decreases, reaches zero (in the top half of the snowpack, the exact location depending on snow density) and proceeds to negative values. This incidentally raises the possibility that radar waves with a certain relative penetration depth may allow the estimation of SIT without requiring any knowledge of the snow

440 depth. The result of potential incomplete penetration for our study is that the magnitude of the reported trend and variance underestimations is diminished. Were our investigation based on a similarly long timeseries of lidar freeboards combined with

a snow climatology, one of our conclusions would be that diminishing snow cover is leading to *overestimation* of rates of decline in the marginal seas.

5.3 The Impact of Enhanced Variability from SnowModel-LG

445 When used instead of mW99, SnowModel-LG data increases the interannual variability of $\overline{SIT}$ in the marginal seas by more than 50%. The main way that this occurs is though increasing $\sigma^2_{\overline{Snow}}$ values (Fig. 5). The second and less significant way that $\sigma^2_{\overline{SIT}}$ is increased is through some positive correlations between $\overline{Snow}$ and $\overline{RF}$ values for individual months in some regions (Fig. 6). Because the two timeseries are positively correlated in some cases, $\sigma^2_{\overline{SIT}}$ is increased; for the Marginal Seas region this covariance term makes up around 15% of $\sigma^2_{\overline{SIT}}$ (Fig. 7).

450 While values for interannual variability are given in W99, it was previously impossible to apply those values to either a given year or to fulfil Eq. (5). SnowModel-LG offers similar variability to the SWE statistics given in W99 (Fig. 1), and can generate a yearly timeseries of values. Furthermore it can be combined with radar freeboard data to generate all terms of Eq. (5) for a direct calculation of $\sigma^2_{\overline{SIT}}$.

Comparing our IAV values to the literature is challenging due to differences in the area over which other authors have 455 calculated IAV values. Haas (2004) investigated the interannual variability of an area within the Transpolar Drift in the Central Arctic and Northern Barents Sea, and found a 0.73 m standard deviation. This is considerably higher than the values determined in this study, although this data was collected by EM sounding in late summer over a ten year period that does not overlap with this analysis. Laxon et al. (2003) defined a 'region of coverage', which essentially consisted of the marginal seas considered in this analysis with the addition of some areas of the Canadian Archipelago and the Greenland sea. The authors found a 460 variability of 0.24 m using W99 in this region of coverage over an eight year timescale. Unlike Haas (2004), this value is lower than our findings using either mW99 or SnowModel-LG. Similar to Haas (2004), the time period is considerably shorter and the geographical area is not identical. Finally, Rothrock et al. (2008) found interannual variability in SIT to be 0.46 m over a twenty-five year period (1975-2000), using submarine records from a variety of Arctic regions. It is likely that the values in these studies differ due to the unequal spatial extent over which the IAV was calculated; averaging over a larger area reduces 465 the IAV due to the averaging out of local anomalies.

5.4 The Impact of New and Steeper Trends in Mean Sea Ice Thickness

The replacement of multiyear ice with first year ice has been documented to be reducing Arctic-mean SWE on sea ice in spring (Webster et al., 2014). However, progressively later freeze-ups in the Arctic are also likely driving a reduction in mean SWE in the early cold-season. This is because ice covers a relatively smaller area in the high precipitation months of September and 470 October. When the ice area then expands with the progression of the growth-season, the newer ice has not been exposed to this snowfall. This mechanism is not accounted for in mW99, and as such snow depths do not decrease at a statistically significant level in any month.

In this study we have assessed how these negative trends in $\overline{Snow}$ propagate through into trends in $\overline{SIT}$. In every area where a statistically significant decline in radar freeboards is observed, a statistically significant decline in SnowModel-LG SWE is

475 also observed (Fig. S16). In addition to this, SnowModel-LG also exhibits $\overline{Snow}$ decline in other months in the Beaufort and Barents Sea. As such, reductions in $\overline{Snow}$ usually act in concert with observed reductions in $\overline{RF}$, amplifying decline in $\overline{SIT}$. This relationship is illustrated by the fact that several months in several regions do not exhibit either a statistically significant decline in $\overline{RF}$ or $\overline{Snow}$ (Fig. S16), but despite this they do exhibit decline in $\overline{SIT}$ (Fig. 9). We note here that this 'co-decline' in $\overline{Snow}$ and $\overline{RF}$ is separate to the covariability presented in Sect. 4.1 and Fig. 6, as that was calculated from detrended data.

480 Because SnowModel-LG data features a steeper decline in $\overline{Snow}$ than mW99, a steeper decline is observed in the $\overline{SIT}$ of several regions. However, SnowModel-LG $\overline{Snow}$ contribution to $\overline{SIT}$ also exhibits significantly more variability, which acts to reduce statistical significance of $\overline{SIT}$ trends. Despite this compensating effect, the statistical significance of trends in $\overline{SIT}$ were generally greater than those calculated using mW99. Furthermore, statistically significant trends emerged in new months and new regions.

485 Kwok and Rothrock (2009) analysed 42 years of submarine records and the five year ICESat record. However, it is challenging to draw comparison with our results, as trends were gleaned from submarine track crossings and by comparing the thickness difference between the period of submarine observation and that of ICESat observations. Difficulty in comparison is further compounded by differences in regional designation and the area of the submarine data release (which is generally confined to the Central Arctic region where the radar altimetry timeseries is truncated). This is also the case for the updated

490 analysis of Kwok (2018), who seasonally adjusted mean thickness values to match crossover points in submarine tracks in time and space.

Our findings of enhanced interannual variability and steeper decline have implications for Arctic stakeholders and the deployment of human infrastructure. The marginal seas are heavily used for the shipping of goods along the Northern Sea Route in summer (Eguíluz et al., 2016) and provide the setting for potential extraction of natural resources (Petrick et al., 2017).

495 Furthermore, the season during which vessels may traverse the Northern Sea Route is lengthening. Higher variability in sea ice thickness may pose a challenge to the planning of this seasonal travel, particularly with regard to the need for ice-strengthened escorts for conventional vessels (Melia et al., 2017; Cariou et al., 2019). The enhancement of declining trends where they exist is perhaps a positive for these industries.

5.5 The interannual relationship between freeboard and snow depth

500 We finally consider the physical mechanisms behind positive or non-significant correlations between $\overline{Snow}$ and $\overline{RF}$ displayed in Fig. (6). Assuming total radar penetration of the snow cover, as snow accumulates on sea ice it should lower the local radar freeboard by a distance on the order of half its accumulated height (Eq. 3). This lowering is a result of physical depression of the ice surface and an increase in the radar ranging due to slower radar wave propagation in snow (in approximately a 60:40 ratio). Over short time scales (days to weeks), this would result in a negative correlation between local snow depth and

505 local radar freeboard; this is not seen. Furthermore, snow is a highly insulating material and its accumulation limits sea ice thermodynamic growth. This would also bring about a negative correlation between snow depth and radar freeboard, lagged over a period of weeks.

The lack of negative correlations between $\overline{RF}$ and $\overline{Snow}$ from year to year is likely indicative of the timescale of our analysis. If present, the negative correlation implied by Eq. (3) and the mechanisms above must only be present on shorter

510 timescales (e.g. days). So what drives the positive correlations between $\overline{RF}$ and $\overline{Snow}$ where they exist? One driver over FYI is likely ice age. Ice formed at the beginning of the season has longer to (a) grow thicker, and (b) accumulate snow. Both variables are therefore likely controlled by regional freeze-up timing, explaining the correlation. The combined evolution of $\overline{Snow}$ and $\overline{RF}$ anomalies as a function of regional freeze-up timings is likely to be the subject of future study. Freeze-up timing perhaps also drives the correlations between $\overline{RF}$ and $\overline{Snow}$ over MYI (where they exist; Fig. S7) via a melt-pond

515 related mechanism. A later freeze-up would cause more snow in the high precipitation months to fall into melt-ponds and therefore not accumulate, although it is difficult to conceive of this mechanism alone driving the observed correlations. The relationship between MYI radar freeboards and accumulated SWE may also form an avenue for further study.

6   Summary

In this paper we used a novel approximation for the slowing of radar waves in snow to decompose the conventional method for

520 estimating sea ice thickness into two contributions: one originating from radar freeboard data (from satellite altimeters), the other from snow data of varying provenance.

This allowed a regional assessment of the conventional impact of snow on variability and trends in sea ice thickness. We then used a new snow data set (from SnowModel-LG) with a more realistic magnitude of interannual variability and trends to calculate the regional sea ice thickness timeseries.

525 We found that interannual variability in average sea ice thickness ($\sigma^2_{\overline{SIT}}$) of the marginal seas was increased by more than 50% by accounting for variability in the snow cover. On a seasonal timescale we find that variability in the snow cover makes an increasing contribution to the total variability of inferred sea ice thickness, increasing from around 20% in October to more than 70% in April.

We also observed that the trends in SnowModel-LG data propagated through to the SIT timeseries, amplifying decline in

530 regions where it was already significant, and introducing significant decline where it did not previously exist. This occurred in spite of the compensating effect of enhanced interannual variability.

Author contributions. JCS, JCL, MT and RW proposed and conceptualised the study. VN provided extensive feedback on the first draft. GEL provided the SnowModel-LG data. RDCM carried out the main analysis. All authors contributed to the write-up.

Code and data availability. The code used for all analysis and visualisation was written in Python 3.6 and is available at

535 github.com/robbiemallett/SnowModel-LG_SIT_Impacts. The radar freeboard data from Envisat and CryoSat-2 is available from the ESA CCI initiative at climate.esa.int/en/odp/#/project. The NESOSIM snow data is available from the NASA Cryospheric Sciences Laboratory

website at earth.gsfc.nasa.gov/cryo/data/nasa-eulerian-snow-sea-ice-model-nesosim. It is anticipated that the SnowModel-LG data will be hosted in a persistent data repository in the near future. Code and data last accessed 2020/9/20.

Competing interests. The authors declare no competing interests.

540 *Acknowledgements.* This work was funded primarily by the London Natural Environmental Research Council Doctoral Training Partnership grant (NE/L002485/1). JCL acknowledges support from the European Space Agency Living Planet Fellowship 'Arctic-SummIT' under grant ESA/4000125582/18/I-NS and the Natural Environmental Research Council Project 'Diatom-ARCTIC' under Grant NE/R012849/1. MT acknowledges support from the European Space Agency in part by project 'Polarice' under grant ESA/AO/1-9132/17/NL/MP and in part by the project 'CryoSat + Antarctica' under Grant ESA AO/1-9156/17/I-BG.

References

Armitage, T. W. and Ridout, A. L.: Arctic sea ice freeboard from AltiKa and comparison with CryoSat-2 and Operation IceBridge, Geophysical Research Letters, 42, 6724–6731, https://doi.org/10.1002/2015GL064823, 2015.

Barrett, A. P., Stroeve, J. C., and Serreze, M. C.: Arctic Ocean Precipitation From Atmospheric Reanalyses and Comparisons With North Pole Drifting Station Records, Journal of Geophysical Research: Oceans, 125, https://doi.org/10.1029/2019JC015415, https://onlinelibrary.wiley.com/doi/abs/10.1029/2019JC015415, 2020.

Beaven, S. G., Lockhart, G. L., Gogineni, S. P., Hosseinmostafa, A. R., Jezek, K., Gow, A. J., Perovich, D. K., Fung, A. K., and Tjuatja, S.: Laboratory measurements of radar backscatter from bare and snow-covered saline ice sheets, International Journal of Remote Sensing, 16, 851–876, https://doi.org/10.1080/01431169508954448, 1995.

Blockley, E. W. and Peterson, K. A.: Improving Met Office seasonal predictions of Arctic sea ice using assimilation of CryoSat-2 thickness, The Cryosphere, 12, 3419–3438, https://doi.org/10.5194/tc-12-3419-2018, https://www.the-cryosphere.net/12/3419/2018/, 2018.

Boisvert, L. N., Webster, M. A., Petty, A. A., Markus, T., Bromwich, D. H., and Cullather, R. I.: Intercomparison of precipitation estimates over the Arctic ocean and its peripheral seas from reanalyses, Journal of Climate, 31, 8441–8462, https://doi.org/10.1175/JCLI-D-18-0125.1, http://journals.ametsoc.org/doi/10.1175/JCLI-D-18-0125.1, 2018.

Brodzik, M. J., Billingsley, B., Haran, T., Raup, B., and Savoie, M. H.: EASE-Grid 2.0: Incremental but Significant Improvements for Earth-Gridded Data Sets, ISPRS International Journal of Geo-Information, 1, 32–45, https://doi.org/10.3390/ijgi1010032, http://www.mdpi.com/2220-9964/1/1/32, 2012.

Bunzel, F., Notz, D., and Pedersen, L. T.: Retrievals of Arctic Sea-Ice Volume and Its Trend Significantly Affected by Interannual Snow Variability, Geophysical Research Letters, 45, 751–11, https://doi.org/10.1029/2018GL078867, 2018.

Cariou, P., Cheaitou, A., Faury, O., and Hamdan, S.: The feasibility of Arctic container shipping: the economic and environmental impacts of ice thickness, Maritime Economics and Logistics, pp. 1–17, https://doi.org/10.1057/s41278-019-00145-3, https://doi.org/10.1057/s41278-019-00145-3, 2019.

Chandler, R. E. and Scott, E. M.: Statistical Methods for Trend Detection and Analysis in the Environmental Sciences, https://doi.org/10.1002/9781119991571, 2011.

Chevallier, M. and Salas-Mélia, D.: The Role of Sea Ice Thickness Distribution in the Arctic Sea Ice Potential Predictability: A Diagnostic Approach with a Coupled GCM, Journal of Climate, 25, 3025–3038, https://doi.org/10.1175/JCLI-D-11-00209.1, http://journals.ametsoc.org/doi/10.1175/JCLI-D-11-00209.1, 2012.

Comiso, J.: Bootstrap Sea Ice Concentrations from Nimbus-7 SMMR and DMSP SSM/I, National Snow and Ice Data Center, Boulder, Colorado. Digital media, 2000.

Eguíluz, V. M., Fernández-Gracia, J., Irigoien, X., and Duarte, C. M.: A quantitative assessment of Arctic shipping in 2010-2014, Scientific Reports, 6, 1–6, https://doi.org/10.1038/srep30682, www.nature.com/scientificreports, 2016.

Giles, K. A., Laxon, S. W., and Ridout, A. L.: Circumpolar thinning of Arctic sea ice following the 2007 record ice extent minimum, Geophysical Research Letters, 35, L22 502, https://doi.org/10.1029/2008GL035710, http://doi.wiley.com/10.1029/2008GL035710, 2008a.

Giles, K. A., Laxon, S. W., and Worby, A. P.: Antarctic sea ice elevation from satellite radar altimetry, Geophysical Research Letters, 35, L03 503, https://doi.org/10.1029/2007GL031572, http://doi.wiley.com/10.1029/2007GL031572, 2008b.

580 Haas, C.: Late-summer sea ice thickness variability in the Arctic Transpolar Drift 1991-2001 derived from ground-based electro-
magnetic sounding, Geophysical Research Letters, 31, n/a–n/a, https://doi.org/10.1029/2003GL019394, http://doi.wiley.com/10.1029/
2003GL019394, 2004.

Hendricks, S. and Ricker, R.: Product User Guide & Algorithm Specification: AWI CryoSat-2 Sea Ice Thickness (version 2.2), 2019.

Hendricks, S., Paul, S., and Rinne, E.: Northern hemisphere sea ice thickness from the CryoSat-2 satellite on a monthly grid (L3C), v2.0,
585 https://doi.org/10.5285/ff79d140824f42dd92b204b4f1e9e7c2, 2018.

Katlein, C., Arndt, S., Nicolaus, M., Perovich, D. K., Jakuba, M. V., Suman, S., Elliott, S., Whitcomb, L. L., McFarland, C. J., Gerdes, R.,
Boetius, A., and German, C. R.: Influence of ice thickness and surface properties on light transmission through <scp>A</scp> rctic sea
ice, Journal of Geophysical Research: Oceans, 120, 5932–5944, https://doi.org/10.1002/2015JC010914, https://onlinelibrary.wiley.com/
doi/abs/10.1002/2015JC010914, 2015.

590 Kern, S., Khvorostovsky, K., Skourup, H., Rinne, E., Parsakhoo, Z. S., Djepa, V., Wadhams, P., and Sandven, S.: The impact of snow depth,
snow density and ice density on sea ice thickness retrieval from satellite radar altimetry: Results from the ESA-CCI Sea Ice ECV Project
Round Robin Exercise, Cryosphere, 9, 37–52, https://doi.org/10.5194/tc-9-37-2015, 2015.

Kurtz, N. T. and Farrell, S. L.: Large-scale surveys of snow depth on Arctic sea ice from Operation IceBridge, Geophysical Research Letters,
38, n/a–n/a, https://doi.org/10.1029/2011GL049216, http://doi.wiley.com/10.1029/2011GL049216, 2011.

595 Kurtz, N. T., Galin, N., and Studinger, M.: An improved CryoSat-2 sea ice freeboard retrieval algorithm through the use of waveform fitting,
Cryosphere, 8, 1217–1237, https://doi.org/10.5194/tc-8-1217-2014, https://www.the-cryosphere.net/8/1217/2014/, 2014.

Kwok, R.: Arctic sea ice thickness, volume, and multiyear ice coverage: Losses and coupled variability (1958-2018), Environmental Research
Letters, 13, 105 005, https://doi.org/10.1088/1748-9326/aae3ec, https://doi.org/10.1088/1748-9326/aae3ec, 2018.

Kwok, R. and Cunningham, G. F.: Variability of arctic sea ice thickness and volume from CryoSat-2, Philosophical Transactions of the Royal
600 Society A: Mathematical, Physical and Engineering Sciences, 373, https://doi.org/10.1098/rsta.2014.0157, 2015.

Kwok, R. and Rothrock, D. A.: Decline in Arctic sea ice thickness from submarine and ICESat records: 1958-2008, Geophysical Research
Letters, 36, https://doi.org/10.1029/2009GL039035, 2009.

Kwok, R., Kacimi, S., Webster, M. A., Kurtz, N. T., and Petty, A. A.: Arctic Snow Depth and Sea Ice Thickness From ICESat-2 and CryoSat-2
Freeboards: A First Examination, Journal of Geophysical Research: Oceans, 125, 1–19, https://doi.org/10.1029/2019JC016008, 2020.

605 Landy, J. C., Petty, A. A., Tsamados, M., and Stroeve, J. C.: Sea ice roughness overlooked as a key source of uncertainty in CryoSat-2 ice
freeboard retrievals, Journal of Geophysical Research: Oceans, 44, 1–36, https://doi.org/10.1029/2019jc015820, 2020.

Laxon, S., Peacock, H., and Smith, D.: High interannual variability of sea ice thickness in the Arctic region, Nature, 425, 947–950,
https://doi.org/10.1038/nature02050, 2003.

Laxon, S. W., Giles, K. A., Ridout, A. L., Wingham, D. J., Willatt, R., Cullen, R., Kwok, R., Schweiger, A., Zhang, J., Haas, C., Hendricks,
610 S., Krishfield, R., Kurtz, N., Farrell, S., and Davidson, M.: CryoSat-2 estimates of Arctic sea ice thickness and volume, Geophysical
Research Letters, 40, 732–737, https://doi.org/10.1002/grl.50193, 2013.

Liston, G. E., Itkin, P., Stroeve, J., Tschudi, M., Stewart, J. S., Pedersen, S. H., Reinking, A. K., and Elder, K.: A Lagrangian
Snow-Evolution System for Sea-Ice Applications (SnowModel-LG): Part I – Model Description, Journal of Geophysical Research:
Oceans, https://doi.org/10.1029/2019jc015913, https://agupubs.onlinelibrary.wiley.com/doi/full/10.1029/2019JC015913https://agupubs.
615 onlinelibrary.wiley.com/doi/abs/10.1029/2019JC015913https://agupubs.onlinelibrary.wiley.com/doi/10.1029/2019JC015913, 2020.

Mallett, R. D., Lawrence, I. R., Stroeve, J. C., Landy, J. C., and Tsamados, M.: Brief communication: Conventional assumptions involving the speed of radar waves in snow introduce systematic underestimates to sea ice thickness and seasonal growth rate estimates, Cryosphere, 14, 251–260, https://doi.org/10.5194/tc-14-251-2020, 2020.

Markus, T., Stroeve, J. C., and Miller, J.: Recent changes in Arctic sea ice melt onset, freezeup, and melt season length, Journal of Geophysical Research: Oceans, 114, https://doi.org/10.1029/2009JC005436, 2009.

Melia, N., Haines, K., Hawkins, E., and Day, J. J.: Towards seasonal Arctic shipping route predictions, Environmental Research Letters, 12, 084 005, https://doi.org/10.1088/1748-9326/aa7a60, https://doi.org/10.1088/1748-9326/aa7a60, 2017.

Meredith, M., Sommerkorn, M., Cassotta, S., Derksen, C., Ekaykin, A., Hollowed, A., Kofinas, G., Mackintosh, A., Melbourne-Thomas, J., Muelbert, M., Ottersen, G., Pritchard, H., and Schuur, E.: Polar Regions, in: IPCC Special Report on the Ocean and Cryosphere in a Changing Climate, edited by Portner, H.-O., Roberts, D., Masson-Delmotte, V., Zhai, P., Tignor, M., Poloczanska, E., Mintenbeck, K., Alegria, A., Nicolai, M., Okem, A., Petzold, J., Rama, B., and Weyer, N., pp. 203–320, IPCC, 2019.

Mundy, C. J., Barber, D. G., and Michel, C.: Variability of snow and ice thermal, physical and optical properties pertinent to sea ice algae biomass during spring, Journal of Marine Systems, 58, 107–120, https://doi.org/10.1016/j.jmarsys.2005.07.003, https://linkinghub.elsevier.com/retrieve/pii/S0924796305001417, 2005.

Nandan, V., Geldsetzer, T., Yackel, J., Mahmud, M., Scharien, R., Howell, S., King, J., Ricker, R., and Else, B.: Effect of Snow Salinity on CryoSat-2 Arctic First-Year Sea Ice Freeboard Measurements, Geophysical Research Letters, 44, 419–10, https://doi.org/10.1002/2017GL074506, http://doi.wiley.com/10.1002/2017GL074506, 2017.

Paul, S., Hendricks, S., Ricker, R., Kern, S., and Rinne, E.: Empirical parametrization of Envisat freeboard retrieval of Arctic and Antarctic sea ice based on CryoSat-2: progress in the ESA Climate Change Initiative, The Cryosphere, 12, 2437–2460, https://doi.org/10.5194/tc-12-2437-2018, https://tc.copernicus.org/articles/12/2437/2018/, 2018.

Petrick, S., Riemann-Campe, K., Hoog, S., Growitsch, C., Schwind, H., Gerdes, R., and Rehdanz, K.: Climate change, future Arctic Sea ice, and the competitiveness of European Arctic offshore oil and gas production on world markets, Ambio, 46, 410–422, https://doi.org/10.1007/s13280-017-0957-z, 2017.

Petty, A. A., Holland, M. M., Bailey, D. A., and Kurtz, N. T.: Warm Arctic, Increased Winter Sea Ice Growth?, Geophysical Research Letters, 45, 922–12, https://doi.org/10.1029/2018GL079223, https://onlinelibrary.wiley.com/doi/abs/10.1029/2018GL079223, 2018a.

Petty, A. A., Webster, M., Boisvert, L., and Markus, T.: The NASA Eulerian Snow on Sea Ice Model (NESOSIM) v1.0: Initial model development and analysis, Geoscientific Model Development, 11, 4577–4602, https://doi.org/10.5194/gmd-11-4577-2018, 2018b.

Quartly, G. D., Rinne, E., Passaro, M., Andersen, O. B., Dinardo, S., Fleury, S., Guillot, A., Hendricks, S., Kurekin, A. A., Müller, F. L., Ricker, R., Skourup, H., and Tsamados, M.: Retrieving sea level and freeboard in the Arctic: A review of current radar altimetry methodologies and future perspectives, https://doi.org/10.3390/RS11070881, 2019.

Ricker, R., Hendricks, S., Helm, V., Skourup, H., and Davidson, M.: Sensitivity of CryoSat-2 Arctic sea-ice freeboard and thickness on radar-waveform interpretation, Cryosphere, 8, 1607–1622, https://doi.org/10.5194/tc-8-1607-2014, https://www.the-cryosphere.net/8/1607/2014/, 2014.

Rösel, A., Itkin, P., King, J., Divine, D., Wang, C., Granskog, M. A., Krumpen, T., and Gerland, S.: Thin Sea Ice, Thick Snow, and Widespread Negative Freeboard Observed During N-ICE2015 North of Svalbard, Journal of Geophysical Research: Oceans, 123, 1156–1176, https://doi.org/10.1002/2017JC012865, 2018.

Rothrock, D. A., Percival, D. B., and Wensnahan, M.: The decline in arctic sea-ice thickness: Separating the spatial, annual, and interannual variability in a quarter century of submarine data, Journal of Geophysical Research: Oceans, 113, https://doi.org/10.1029/2007JC004252,

https://agupubs.onlinelibrary.wiley.com/doi/full/10.1029/2007JC004252https://agupubs.onlinelibrary.wiley.com/doi/abs/10.1029/
2007JC004252https://agupubs.onlinelibrary.wiley.com/doi/10.1029/2007JC004252, 2008.

Sallila, H., Farrell, S. L., McCurry, J., and Rinne, E.: Assessment of contemporary satellite sea ice thickness products for Arctic sea ice, The Cryosphere, 13, 1187–1213, https://doi.org/10.5194/tc-13-1187-2019, https://www.the-cryosphere.net/13/1187/2019/, 2019.

Schröder, D., Feltham, D. L., Tsamados, M., Ridout, A., and Tilling, R.: New insight from CryoSat-2 sea ice thickness for sea ice modelling, The Cryosphere, 13, 125–139, https://doi.org/10.5194/tc-13-125-2019, https://www.the-cryosphere.net/13/125/2019/, 2019.

Schweiger, A. J., Wood, K. R., and Zhang, J.: Arctic Sea Ice volume variability over 1901-2010: A model-based reconstruction, Journal of Climate, 32, 4731–4752, https://doi.org/10.1175/JCLI-D-19-0008.1, 2019.

Stroeve, J. and Notz, D.: Changing state of Arctic sea ice across all seasons, Environmental Research Letters, 13, 103 001, https://doi.org/10.1088/1748-9326/aade56, https://doi.org/10.1088/1748-9326/aade56, 2018.

Stroeve, J., Liston, G. E., Buzzard, S., Zhou, L., Mallett, R., Barrett, A., Tschudi, M., Tsamados, M., Itkin, P., and Stewart, J. S.: A Lagrangian Snow-Evolution System for Sea Ice Applications (SnowModel-LG): Part II - Analyses, Journal of Geophysical Research: Oceans, https://doi.org/10.1029/2019JC015900, https://onlinelibrary.wiley.com/doi/abs/10.1029/2019JC015900, 2020.

Stroeve, J. C., Markus, T., Boisvert, L., Miller, J., and Barrett, A.: Changes in Arctic melt season and implications for sea ice loss, Geophysical Research Letters, 41, 1216–1225, https://doi.org/10.1002/2013GL058951, http://doi.wiley.com/10.1002/2013GL058951, 2014.

Tilling, R. L., Ridout, A., and Shepherd, A.: Estimating Arctic sea ice thickness and volume using CryoSat-2 radar altimeter data, Advances in Space Research, 62, 1203–1225, https://doi.org/10.1016/j.asr.2017.10.051, https://doi.org/10.1016/j.asr.2017.10.051, 2018.

Tsamados, M., Feltham, D. L., and Wilchinsky, A. V.: Impact of a new anisotropic rheology on simulations of Arctic Sea ice, Journal of Geophysical Research: Oceans, 118, 91–107, https://doi.org/10.1029/2012JC007990, 2013.

Vella, D. and Wettlaufer, J. S.: Explaining the patterns formed by ice floe interactions, Journal of Geophysical Research, 113, C11 011, https://doi.org/10.1029/2008JC004781, http://doi.wiley.com/10.1029/2008JC004781, 2008.

Warren, S. G., Rigor, I. G., Untersteiner, N., Radionov, V. F., Bryazgin, N. N., Aleksandrov, Y. I., and Colony, R.: Snow depth on Arctic sea ice, Journal of Climate, 12, 1814–1829, https://doi.org/10.1175/1520-0442(1999)012<1814:SDOASI>2.0.CO;2, 1999.

Webster, M. A., Rigor, I. G., Nghiem, S. V., Kurtz, N. T., Farrell, S. L., Perovich, D. K., and Sturm, M.: Interdecadal changes in snow depth on Arctic sea ice, Journal of Geophysical Research: Oceans, 119, 5395–5406, http://doi.wiley.com/10.1002/2014JC009985, 2014.

Willatt, R., Laxon, S., Giles, K., Cullen, R., Haas, C., and Helm, V.: Ku-band radar penetration into snow cover on Arctic sea ice using airborne data, Annals of Glaciology, 52, 197–205, https://doi.org/10.3189/172756411795931589, 2011.

Willatt, R. C., Giles, K. A., Laxon, S. W., Stone-Drake, L., and Worby, A. P.: Field investigations of Ku-band radar penetration into snow cover on antarctic sea ice, IEEE Transactions on Geoscience and Remote Sensing, 48, 365–372, https://doi.org/10.1109/TGRS.2009.2028237, http://ieeexplore.ieee.org/document/5282596/, 2010.

Zygmuntowska, M., Rampal, P., Ivanova, N., and Smedsrud, L. H.: Uncertainties in Arctic sea ice thickness and volume: New estimates and implications for trends, Cryosphere, 8, 705–720, https://doi.org/10.5194/tc-8-705-2014, https://www.the-cryosphere.net/8/705/2014/, 2014.